Cytotechnology **24:** 121–134, 1997.

Investigations on oxygen limitations of adherent cells growing on macroporous microcarriers

A. Preissmann[1], R. Wiesmann[2], R. Buchholz[3], R. G. Werner[1] & W. Noé[1]
[1] *Dr. Karl Thomae GmbH (Boehringer Ingelheim), Department of Biotechnical Production, Birkendorfer Str. 65, 88397 Biberach/Riss;* [2] *Bioverfahrenstechnik GbR, Seestr. 13, 10553 Berlin;* [3] *Technical University of Berlin, Institute for Biotechnology, Department of Bioprocess Engineering, Ackerstr. 71–76, 13355 Berlin*

Received 5 September 1995; accepted 27 February 1996

Key words: dissolved oxygen profile, fibroblasts, fluidized bed, macroporous carrier, oxygen microprobe, recombinantC–127

Abstract

Macroporous microcarriers are commonly applied to fixed and fluidized bed bioreactors for the cultivation of stringent adherent cells. Several investigations showed that these carriers are advantageous in respect to a large surface area (Griffiths, 1990; Looby, 1990a).

When growing a rC–127 cell line on Cytoline 2 (Pharmacia Biotech), no satisfactory product yield could be achieved. A possible limitation in the supply of nutrient components was investigated to explain these poor results. No significant concentration gradients could be detected. Nevertheless, fluorescence staining revealed a decreasing viability, particularly inside the macroporous structure. Therefore, oxygen transfer to and into the carriers was examined by means of an oxygen microprobe during the entire process. Additional mathematical modeling supported these results.

The maximum penetration depth of oxygen was determined to be 300 μm. A critical value influencing the oxygen uptake rate of the rC–127 cells occured at a dissolved oxygen concentration of 8% of air saturation. A significant mass transfer resistance within a laminar boundary film at the surface of the carrier could be detected. This boundary layer had a depth of 170 μm. The results showed that even a 40% air saturation in the bulk liquid could not provide an efficient oxygenation of the surface biofilm during the exponential growth phase. Fluorescent staining reveals a poor viability of cells growing *inside* the carrier volume. Thus, oxygen supply limits the growth of rC–127 cells on macroporous microcarriers. Poor process performance and low product yield could be explained this way.

Abbreviations: d_p – diameter of particle; d_R – diameter of reactor; ε_G – relative gas holdup; η_L – dynamic viscosity of the fluid; ν_t – turbulent viscosity; ρ_L – specific gravity of the fluid; Re_{BC} – Reynolds number for bubble columns; Re_p – Reynolds number for particles; u'_{L0} – fluid velocity in the reactor axis; ω_r – relative fluid velocity

Introduction

Most large-scale processes for the production of human proteins are based on stirred tank technology due to its outstanding advantages (Werner, 1988). However, there are still some stringent adherent cell-lines of industrial importance (e.g. C–127, MDBK, Vero) which cannot be cultivated in conventional suspended systems. In designing large-scale processes for adherent cells, there are two major obstacles: first, the cultivation system has to provide a large surface area to achieve high cell densities and a reasonable product yield. Second, there is no direct access to parameters that monitor the physiological status of the cell

and its surrounding environment. In order to control and assess the course of a process, reliable indirect parameters which require a thorough understanding of biochemical links and metabolical activities of each individual cell-line have to be established.

One of the problems was solved by introducing macroporous microcarriers which offer a high surface-to-volume ratio. They can be applied to both, fixed bed and fluidized bed bioreactors (Looby, 1990a). Limitations and low productivity which occured with solid microcarriers can be diminished by a macroporous structure (Looby, 1990b). In addition, fluidized bed bioreactors provide a very high interphase mass transfer since both cells and fluid are moved.

Nevertheless, some questions concerning possible limitations within the porous matrix arose. Kennard and his coworkers observed that after 20 days of cultivating CHO cells of tissue-like densities inside the carrier, the glucose consumption rate decreased as a result of the formation of necrotic cores (Kennard, 1993). Low product yields were explained by critical mass transfer resistances inside the immobilized volume (Bassi, 1991).

Since we obtained a poor product yield from processes using macroporous microcarriers, we tried to assess limiting parameters for cells growing on and within such carriers. A close examination of nutrient components and their gradients throughout the fluidized bed was carried out. Moreover, the dissolved oxygen (DO) profiles near the surface of a cell-laden carrier were registered for detailed information on the availability of oxygen on the surface and within the carrier.

The DO was measured with a microcoaxial needle electrode. This electrode was established by Baumgärtl and Lübbers (Baumgärtl and Lübbers, 1973) and has been used for a variety of scientific inquiries: DO measurements in organs and living tissues (Baumgärtl and Lübbers, 1983), the estimation of oxygen mass transfer from air bubbles into fluids (Riethues, 1986), O_2 partial pressure distribution measurements in penicillium pellets (Wittler, 1986), immobilized systems (Beunink, 1989; Wiesmann, 1994) and biofilms (Özoguz, 1994) are examples of the succesful use of these electrodes in medical and biotechnological applications.

Materials and methods

Cell line, cultivation conditions and properties of the carriers

For all investigations, a recombinant murine fibroblast cell (rC–127) which produces highly glycosylated recombinant human proteins was used. It was cultivated in a 1:1 mixture of DMEM/F12 supplemented with 5% FCS. For the cultivation of the adherent cell line we used Cytoline 2® Carriers (Pharmacia Biotech, Uppsala, Sweden) with a specific gravity ρ of 1.03 g/cm^3 and a size of 0.4 to 2.5 mm in diameter. Cytoline 2 is made of a plastic polymer matrix. The carrier concentration in the reactor was 20% of column volume. Before usage the carriers were pretreated as specified by the manufacturer.

Bioreactor set-up and analytical methods

According to our comparative studies (Preißmann, 1994), a fluidized bed bioreactor maintained via an external loop for oxygenation, pH control and medium exchange, showed most promising characteristics for the cultivation of the rC–127 cell line growing on microcarriers. Therefore, we applied a 1.2 l fluidized bed column for these investigations. During fermentation, microcarrier samples were taken periodically for optical analysis by fluorescent staining and DO measurement. Fluorescent staining was performed according to a method described by Nikolai *et al*. (Nikolai, 1992), using fluoresceindiacetate (FDA, Sigma No. 596–09–8) and ethidiumbromide (EB, Sigma No. 1239–45–8). FDA rapidly crosses the intact membrane of viable cells and is transformed into fluorescein, a green fluorescent dye, by cytoplasmic esterases. Dead cells incorporate red ethidiumbromide, which causes red fluorescence, into the nuclear DNA strands. 0.2 mL of bioreactor sample were washed twice with an equal volume of PBS to remove the medium. After adding 2 mL of the FDA/EB solution to the microcarriers, incubating it for 2–4 min, and washing the carriers twice with PBS, the carriers were immediately examined with an Olympus stereomicroscope, type AHBT, equipped with a camera.

Glucose and lactate concentrations were automatically monitored with a YSI 2700 system (Yellow springs Instruments, Yellow Springs, USA). Ammonia, lactate dehydrogenase (LDH) and glutamine were determined by enzymatic test-kits (Boehringer Mannheim, Mannheim, Germany); the product titre

was analyzed by sandwich ELISA. Amino acid analysis was performed by means of HPLC (OPA method).

In order to enumerate the cells on the carriers, cell nuclei were extracted with a lysis-buffer containing 1.0% Triton X100 in 0.1 M citric acid. After 4 h incubation time at 37 °C and vigorous shaking, the samples were counted in a hemocytometer.

Experimental set-up

The carrier was fixed within a glass airlift reactor (height 130 mm, diameter 30 mm) using an external loop (see Fig. 1). Measurements are performed on a *single carrier under culture conditions in situ.* By changing the location of the aeration from the measurement tube to the external loop, direct and indirect aeration can be simulated. The electrode was moved backwards from the surface of the fixed carrier in defined steps of 10 μm by means of a Hybrid Piezo Manipulator (model PM 500–20, Frankenberger, Gilching). Any movement of the carrier during the approach of the electrode towards the carrier surface was prevented. The mini-airlift reactor was equipped with a stereomicroscope for the optical control of the exact probe position.

Oxygen micro-electrode

Oxygen kinetics near the surface of the carrier were measured polarographically with a membrane-covered microcoaxial needle electrode (Baumgärtl, 1983). A schematic drawing of the electrode is given by Wiesmann (Wiesmann, 1994). A polarisation voltage of 700 mV was generated by a highly insulated diode-stabilized voltage source (MPI, Dortmund, Germany). The current resulting from oxygen reduction is amplified by a nanoamperemeter (type N23/2, Knick, Berlin, Germany) and recorded via a data acquisition unit (type 3497 A, Hewlett Packard, Palo Alto, USA) and an IEEE–488-interface (type KPC–488.2, Keithley Instruments, Taunton, USA) and by a personal computer (AT 8088). Before each measurement, the calibration of the electrode was performed in nitrogen saturated medium and a medium with a saturation of 40% oxygen, gassed with compressed air.

Results

Time course of a typical fermentation run using microcarriers in a fluidized bed column

Figures 2 and 3 show the data of a typical fermentation run for the cultivation of rC–127. Continuous operation lasted from day 3 to day 20. The feed rate was adjusted daily to maintain a constant concentration of nutrients. A limitation of substrates was prevented this way.

In Figure 2 the concentrations of glucose, glutamine, lactate and ammonium and the product titre are shown. During the perfusion period, glucose concentration is kept above a minimum of 1.2 g/L. Also the glutamine level does not fall below 0.14 g/L. According to our experiences, these concentrations are far from a critical concentration for the cells and local concentration gradients should not have any limiting influences on the metabolism of the cells. Thus, a limitation of the main nutrients could be avoided. Additionally, the amino acid analysis proved that no limitations occured in this respect. Toxic metabolites, such as ammonium and lactate, did not exceed a critical level (data not shown). Frequent medium exchanges ensured low concentrations of the toxic metabolites.

Product formation increased up to day 8. Then, the product formation rate started to decrease slightly during the entire cultivation period. Variations of the fermentation parameters, such as feed rate and feed strategy, did not result in optimized product yields. At the end of the process we terminated the medium exchange to investigate limited conditions during the batch phase (see Fig. 2). As expected, product titre, ammonium and lactate concentrations accumulated whereas glucose was consumed completely after 3 days of cultivation.

In Figure 3 the consumption rate of glucose and glutamine, the product formation rate and the cell number are shown. It is obvious that all parameters have almost parallel kinetics. A maximum in the formation- and consumption rate is reached on day 10 whereafter the values slowly decrease.

As the cell number indicates, the cells grow to a maximum density of 3.15×10^6 cells/mL on day 15. Afterwards the cell number drops rapidly. This can be explained by the previous decrease in metabolic activity. Ending the medium exchange triggers a fast decrease in product-formation- and consumption rates.

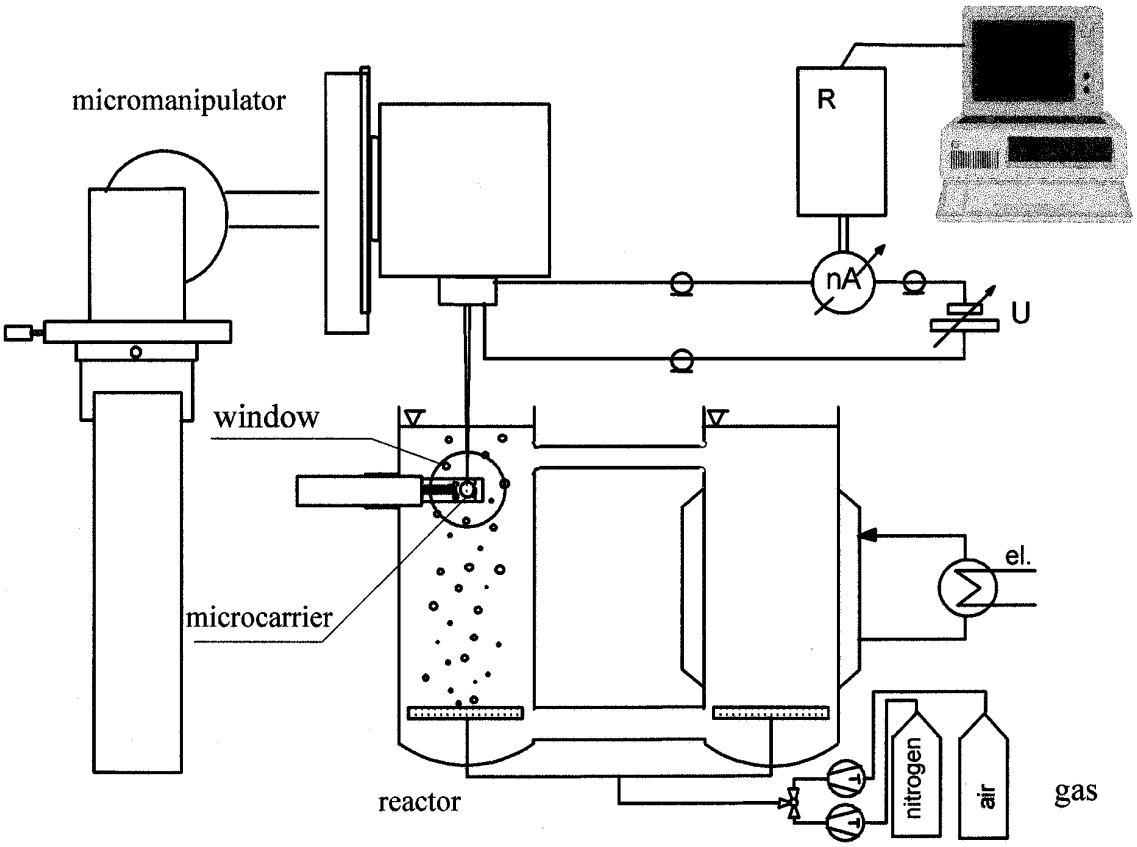

Figure 1. Schematic drawing of the experimental set-up for the measurements of the dissolved oxygen profiles.

Study of concentration gradients regarding the major nutrient components

Throughout the height of the fluidized bed column, sample ports were installed. This way, we investigated axial concentration gradients in the column during the course of the processes. For this purpose, samples were taken simultaneously from the column and from the conditioning vessel. After analyzing the samples, the results were compared with respect to concentration gradients of the major nutrient components. The sampling procedure was repeated daily to assess the influence of increasing cell densities on the nutrient supply and the concentration gradients in the fluidized bed.

Table 1 shows the concentrations of the major nutrient components at different sample ports and at different times during the course of various fermentations. The linear fluid flow rate was also changed in order to investigate the effects of mixing on the nutrient supply.

For all conditions tested in this study, it can be stated that no significant concentration gradients of nutrients occurred throughout the fluidized bed. If deviations occured, they were due to the tolerances of the analyzation methods. Consequently, the fluidized bed system is perfectly capable of maintaining an optimal supply of nutrients and of efficiently removing toxic metabolites.

Assessment of the viability of cells growing on microcarriers by fluorescence staining

Since there is no direct access to cells attached to macroporous microcarriers, it is difficult to obtain information on the physiological state of the cells. The fluorescent staining method used in this study enabled us to differentiate between viable and dead cells *in*

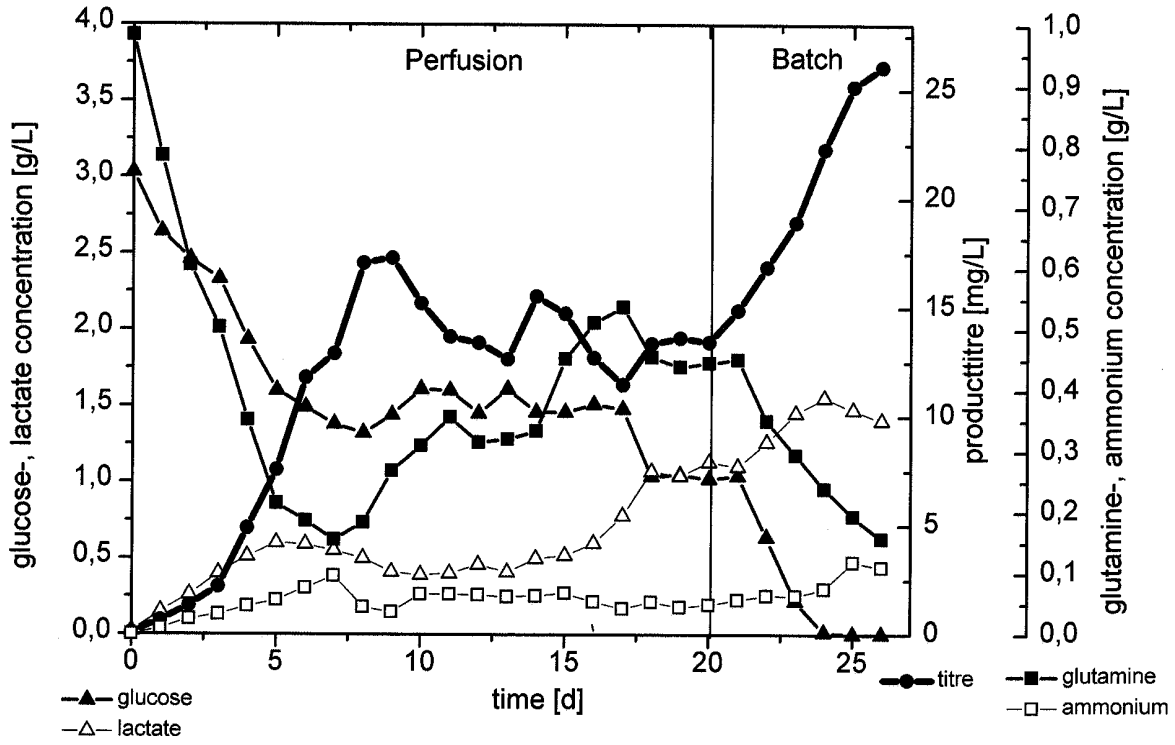

Figure 2. Time course of glucose-, lactate-, glutamine- and ammonium-concentrations and product titre during a fermentation run cultivating rC–127 cells on macroporous microcarriers.

situ. That means that the cells could be examined optically without detachment prior to analysis. Therefore, cell density, morphological features and distribution of cells on the carrier surface were assessed in detail.

Figure 4 shows a photograph of a carrier sampled from a fermentation run 48 h after inoculation. The fluorescent spots, either green or red, represent single cells. It is obvious that the carrier is not yet completely colonized. However, the cell distribution on the carrier seems to be uniform. Staining reveals that up to 95% of the cells are viable in this early stage of the process because almost all cells appear green.

Another carrier sample from day 20 of the same fermentation run shows a decreasing viability (see Fig. 5). After nearly 3 weeks of cultivation, the surface of the carrier is still not completely colonized although cell density has obviously increased. This is indicated by the darker regions lacking any fluorescent spots. This means that cells prefer large pores and deep-seated locations which offer protection against shear stress and collisions of carriers with the vessel wall and with each other. On close examination, it becomes evident that a thin layer of scattered, green-fluorescent, viable cells only occurs near the surface. The poor nutritional condition of the cells beneath this layer is pointed out by the uptake of EB. Even larger agglomerates of dead cells can be found. They are indicated in Figure 5.

All these results coincide with a decrease in metabolic rates of the fermentation runs. A lower viability of the cells results in diminishing metabolic activities. Additional scanning electron microscopy (data not shown) revealed an extended and fibrous morphology of rC–127. The outstretched cells cover even larger pores, forming a sheet-like structure. This morphology has two main disadvantages:

– First, the tissue structure at the carrier surface represents an additional resistance to mass transfer into the carrier volume.
– Second, the cells are inefficiently attached to their matrix by a few anchoring sites at both ends of a cell only. The cell is stretched across the pore volume. Consequently, the matrix of the carrier can not stabilize the cells. So they are exposed to mechanical forces (e.g. in case of collisions).

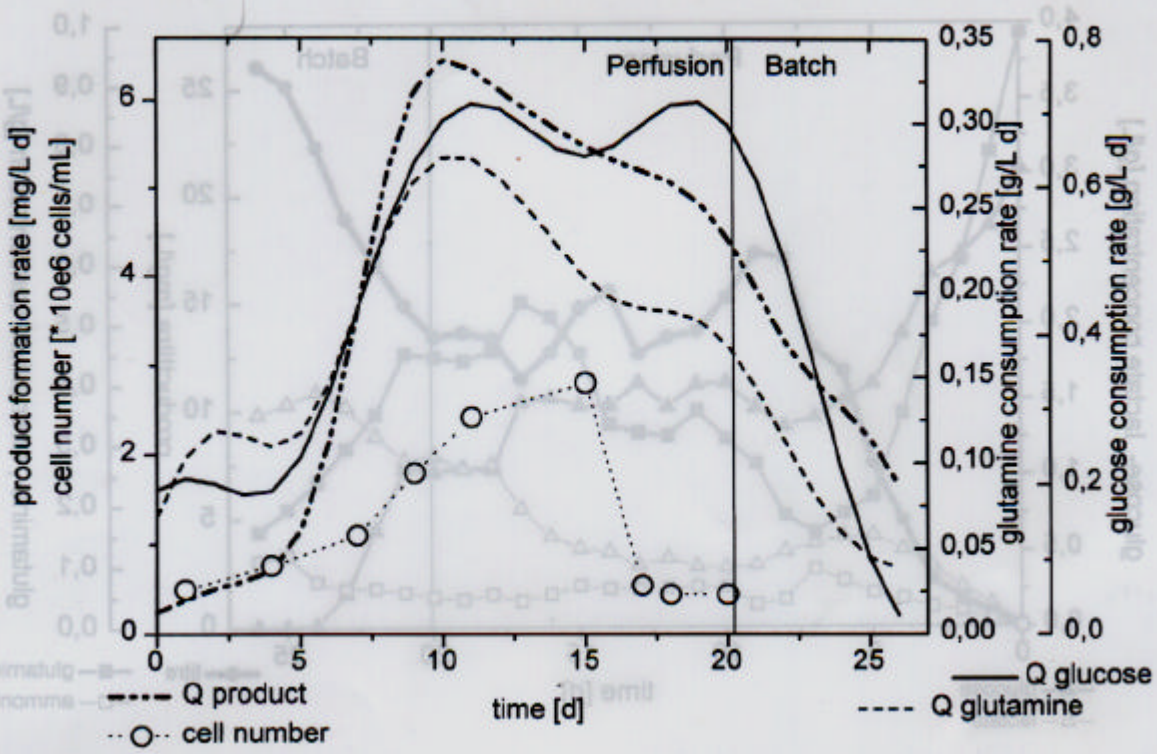

Figure 3. Time course of glucose- and glutamine consumption rate, product formation and cell density during a fermentation run cultivating rC–127 cells on microcarrier.

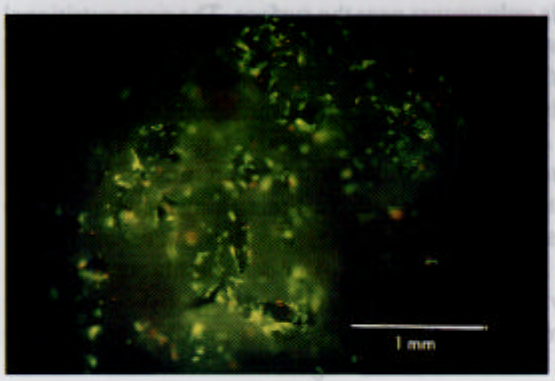

Figure 4. Photograph of a Cytoline carrier stained with FDA/EB. The carrier was sampled on day 2 of fermentation.

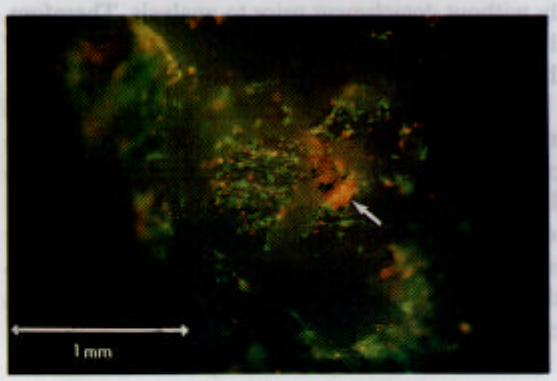

Figure 5. Photograph of a Cytoline carrier stained with FDA/EB. The carrier was sampled on day 20 of fermentation.

Calculation of the hydrodynamic conditions in fermentor and in the measurement apparatus

In order to ensure comparable and reproducible hydrodynamic conditions in both bioreactor and measurement apparatus, the core parameters for the fermentor were determined. Based on these calculations, the fluid flow conditions in the measuring device were adjusted according to those of the bioreactor.

One significant parameter to describe the fluid flow is the Reynolds number. Equation 1 describes the mod-

Table 1. Comparison of the concentrations of metabolites and product in the conditioning vessel and in the fluidized bed column

Run no.	Run time (d)	Sample port ⊗	Recirculation rate (mL/min)	Glucose (g/L)	Lactate (g/L)	Glutamine (mg/L)	Ammonium (mg/L)	Titre (mg/L)
1	14	vessel	1030	3.05	0.17	417	33	1.07
1	14	column (200)	1030	3.04	0.19	423	33	1.06
1	14	column (100)	1030	3.03	0.17	419	32	1.04
1	21	vessel	1245	2.03	0.75	271	53	2.9
1	21	column (100)	1245	2.03	0.72	315	43	1.44
1	29	vessel	1620	1.83	0.72	278	50	1.46
1	29	column (100)	1620	1.73	0.81	261	61	1.89
1	34	vessel	1809	1.78	0.66	275	64	1.69
1	34	column (500)	1809	1.81	0.67	261	62	1.77
1	37	vessel	1809	1.77	0.74	265	69	1.69
1	37	column (500)	1809	1.76	0.74	278	62	1.7
2	17	vessel	1232	2.70	0.15	339	40	4.73
2	17	column (100)	1232	2.61	0.16	337	39	4.14
3	7	vessel	1028	6.14	0.25	466	37	2.01
3	7	column	1028	6.02	0.25	394	39	2.21
3	29	vessel	2046	4.69	0.401	87	92	5.84
3	29	column	2046	4.88	0.509	87	85	6.05
3	41	vessel	2046	2.82	0.467	330	58	4.88
3	41	column	2046	2.86	0.669	224	57	4.94
4	41	vessel	825	1.52	0.866	519	56	6.501
4	41	column	825	1.41	0.869	469	49	6.62

⊗: The numbers in brackets resemble the distance of the sample port from the inlet of the column.

ified Reynolds number for the flow around solid spherical particles.

$$\mathrm{Re}_p = \frac{w_r d_p \rho}{\eta} \quad (1)$$

For the bioreactor we obtained Reynolds numbers in the range of 6 to 75.7 resembling fluid velocities of 2.7×10^{-3} to 25×10^{-3} m/s.

Based on these results we set the same range of Reynolds numbers in the mini airlift reactor. Since the fluid velocitiy in an airlift reactor is determined by the gas flow rate, we calculated the fluid velocity in the axis with the help of Equation 2 (Deckwer,1985; Riquarts, 1981).

$$\mathrm{u}'_{L0} = \frac{1 - 0.75\varepsilon_G}{1 - \varepsilon_G} \frac{\varepsilon_G \, g \, d_{R^2}}{48 \, \nu_t} \quad (2)$$

The gas holdup ε_G is given by

$$\varepsilon_G = \frac{L_g - L_l}{L_g} \quad (3)$$

For the turbulent viscosity, ν_t, Riquarts proposed the following equation.

$$\nu_t = 0.011 d_R \sqrt{d_R g} \left(\frac{u_G^3}{\nu_l g} \right)^{0.125} \quad (4)$$

The superficial gas velocity can be determined by Equation 5

$$\mathrm{u}_G = \frac{\dot{\mathrm{V}}_G}{\frac{\pi}{4} d_R^2} \quad (5)$$

The fluid velocity, u'_{L0}, can be applied to Equation 6 to calculate the Reynolds number for the fluid flow around solid beads.

$$\mathrm{Re} = \frac{\mathrm{u}'_{L0} \, d_p \, \rho}{\eta} \quad (6)$$

According to this calculations we adjusted the Reynolds number in the mini airlift reactor through the gas flow rate to that of the fluidized bed.

Measurement of oxygen-profiles at the surface of colonized carriers

An oxygen microprobe and an experimental set-up of a mini airlift reactor enabled the *in-situ* measurement of

oxygen gradients near the surface and inside the pores of the carrier. For this purpose, samples were taken periodically during a fermentation run (see above) and the oxygen measurements ensued immediately. A typical oxygen profile near the surface of a carrier sampled on day 5 of the culture is shown in Figure 6.

According to the film theory (Whitman, 1923), the oxygen concentration decreases almost linearly within a laminar boundary layer. Repeated experiments on various locations of the carrier proved this layer to have a depth of 170 μm. The oxygen profiles were perfectly reproducible with only slight deviations due to the irregular distribution of cells. In this trial, the DO concentration in the bulk of the fluid was set at a constant concentration of 40% of air saturation. At the surface of the carrier only 14% DO could be detected. This leads to the conclusion that a bulk concentration of 40%, a standard operation condition for these fermentations, is not capable to supply all cells in the exponential growth phase sufficiently with O_2. These values, concerning cells growing directly on the surface of carriers, raised the question of a supply bottleneck inside the pores. Measurements were carried out to obtain further information.

A critical value of DO for the rC–127 cells was detected with the help of dynamic OUR measurements. As shown in Figure 7 the linear decrease in DO drops significantly below a DO concentration of 8%.

Figure 8 depicts the oxygen concentration inside a pore of the carrier. A microprobe was carefully inserted into a pore and was then withdrawn in defined steps to avoid artifacts during the reading. Before this procedure, the microprobe was carefully moved to the surface of the carrier. With the help of a stereomicroscope the exact postion was optically controlled and the micromanipulator was set to zero. The maximum penetration depth of oxygen for rC–127 cells growing on Cytoline carrier is 300 μm. At this point, the oxygen concentration was reduced to zero. The slight increase in DO at a penetration depth of around 110 μm can be explained by an artificial membrane pressure caused during penetration of the carrier matrix. The constant plateau at the surface and 60 μm inside the carrier is apparently caused by the cell layer. The DO profile outside the carrier perfectly matches that of the other experiments and shows a boundary layer of 170 μm. The scattering of the data starts to increase when the probe leaves the laminar film around the particle and enters the turbulent liquid bulk (see Fig. 8).

On day 7 of the cultivation, the boundary film thickness was reduced to 60 μm (see Fig. 6). The oxygen gradient and, consequently, the uptake rate had decreased. The experiments were conducted using 40% of air saturation as bulk liquid oxygen concentration. At the carrier surface a dissolved oxygen concentration of 17% could be detected. Since this value is rather low an oxygen limited region inside the carrier was most probable.

Although we tried to keep the hydrodynamic conditions constant, the boundary film depth is influenced by deviations in the fluid flow around the carrier. The carriers were not exactly of the same size and shape.

On day 17 of the fermentation run, the oxygen uptake had dropped even more (see Fig. 6). The gradient within the boundary layer of again 60 μm had decreased so that 26% of air saturation were detected at the carrier surface. The measurements on day 20 revealed that the oxygen uptake rate had dropped again. The concentration gradient near the particle surface decreased. Comparable results were found on day 24, four days after termination of the medium exchange.

Mathematical describtion of the oxygen transfer from the liquid to the carrier volume

Figure 9 shows the mass transfer of oxygen from the gas phase to the cells in the carrier volume schematically.

Mass transfer gas/liquid from the gas phase to the liquid bulk is not considered here, because the DO concentration in the liquid was controlled at a constant value of 40% of air saturation for all experiments.

When focusing on the transport from liquid to the carrier volume, two mass transfer resistances have to be considered: mass transfer throuogh the boundary layer surrounding the carrier (see Fig. 9: (2)) and diffusion into the carrier volume (see Fig. 9: (3)).

Mass transfer through laminar boundary layers can be described according to Equation 7.

$$q_{O_2} X = k_L a_c (c_{O_2}\text{bulk} - c_{O_2}\text{surface}) \qquad (7)$$

The specific oxygen uptake rate q_{O_2} for rC–127 cells was 8.72 μg $O_2/10^6$ cells h. The cell number X varied during the fermentation runs. The oxygen concentrations in the liquid bulk c_{O_2} bulk and on the carrier surface c_{O_2} surface were measured. The DO concentration of air saturated medium was 6.5 mg/L as proposed by Henzler and Kauling (Henzler and Kauling, 1993). The specific surface of the carriers was calculated by Equation 8 (Kunii and Levenspiel, 1969).

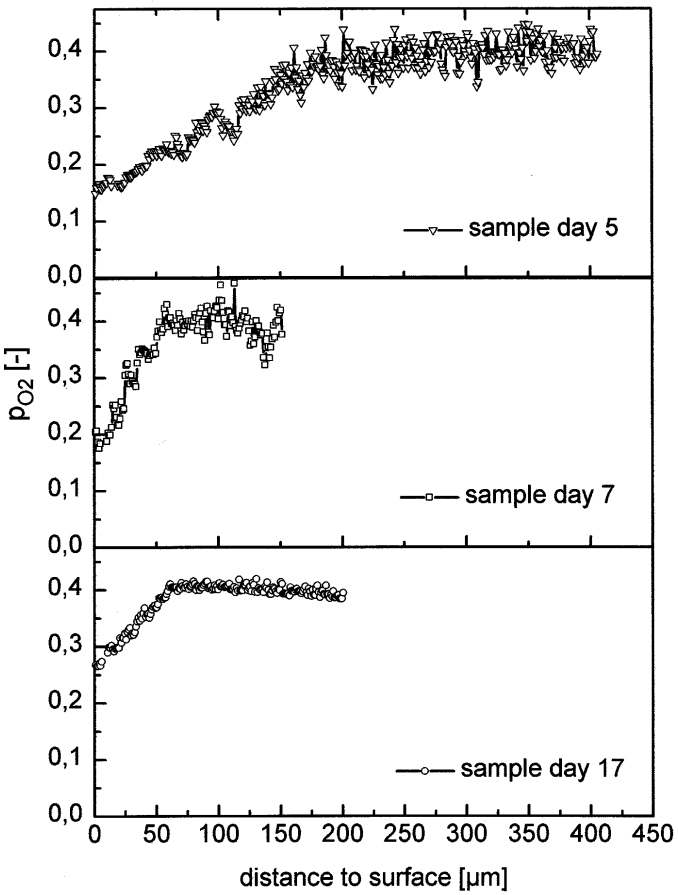

Figure 6. Profiles of dissolved oxygen at the surface of a microcarrier. The carriers were sampled on day 5, 8 and 17 of fermentation.

$$\frac{6(1-\varepsilon)}{\gamma_s d_p} = \frac{\text{surface of particles}}{\text{bed volume}} \tag{8}$$

The transport coefficient k_L can be obtained by a mass transfer model for solid particles introduced by Brauer (Brauer, 1971). The Sherwood number is defined by Equation 9.

$$\frac{k_L D}{d_p} = Sh = 2 + f_k \frac{(\mathrm{Re}Sc)^{1.7}}{1 + (\mathrm{Re}Sc)^{1.2}} \tag{9}$$

where f_K is a function of the Schmidt number

$$f_k = \frac{0.66}{\sqrt[3]{1 + (0.84 Sc^{1/6})}} \tag{10}$$

We compared the results for k_L with the measured data. According to the film theory of Whitman k_L is given by Equation 11.

$$k_L = \frac{D}{\delta} \tag{11}$$

where δ is the thickness of the laminar boundary layer and D the diffusion coefficient for oxygen D = 3.1×10^{-9} m^2/s (H_2O, 37 °C). The measured data gave a mass transfer coefficient of 1.8×10^{-5} m/s with a boundary layer of 170 μm. The theoretical mass transfer model supported these values. The mean deviation of the results was 11%.

The diffusion into the carrier can be described with Equation 12.

$$q_{O_2} X = \left(\frac{\partial^2 r}{\partial r^2} + \frac{2}{r} \frac{\partial c}{\partial r} \right) \tag{12}$$

For a sphere with an anaerobe center the boundary conditions are: $c = c_s$ at $r = r_s$ and c = 0 and dc/dr = 0 at $r = r_s - r_0$. The critical radius r_0 can be approximated by calculating the radius of a sphere in

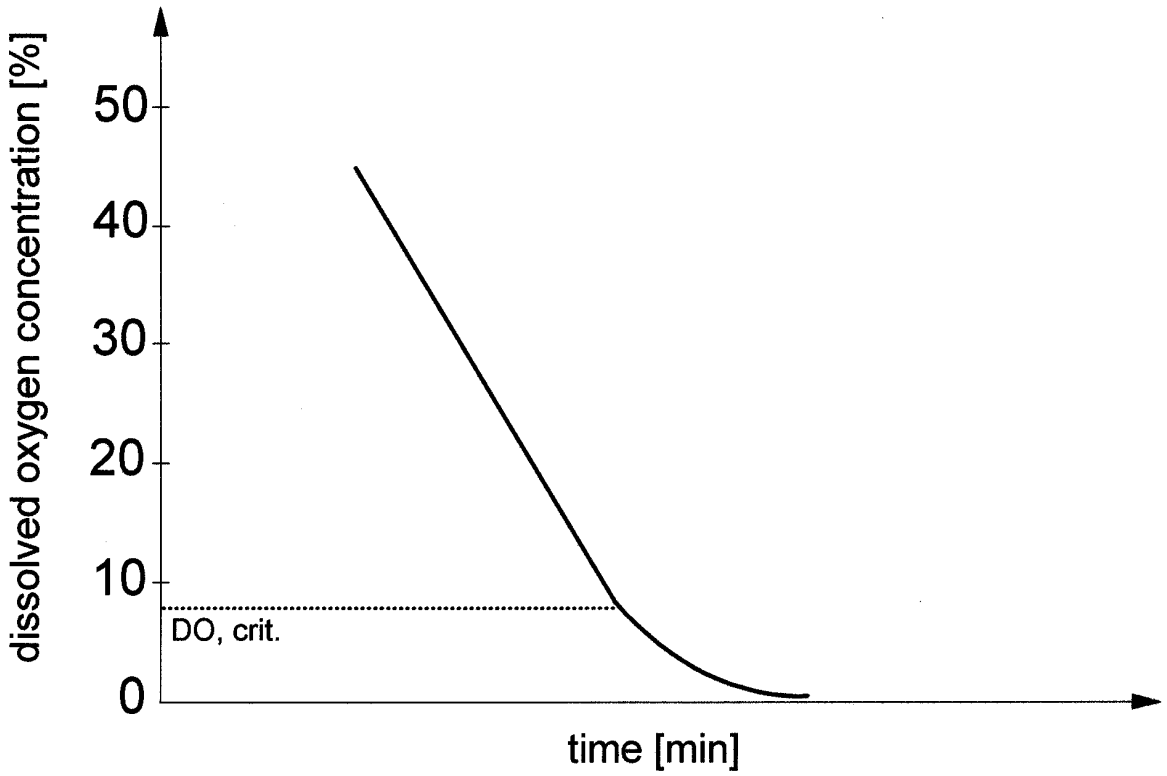

Figure 7. Schematic diagram of dynamic OUR measurement for the determination of the critical DO concentration.

which c is just zero at its centre. The volume to surface ratio of this sphere can then be transferred to the given particle (Murdin, 1988).

$$\text{radius} = \sqrt{\frac{6D\ c_s}{q_{O_2}\ X}} \tag{13}$$

For the estimation of the effective diffusion coefficient in a cell-laden carrier the approach of Westrin and Axelsson can be used (Westrin and Axelsson, 1991). An approximate value of the efficient diffusion coefficient for the void fraction of the carrier D_{e_0} is calculated by Equation 14.

$$\frac{D_{e_0}}{D_{aq}} = \frac{(1-\varphi_p)^3}{(1+\varphi_p)^2} \tag{14}$$

The polymer volume fraction φ_p is defined as $\varphi_p = \frac{\phi_p}{1-\varphi_{\text{cells}}}$ with the polymer volume fraction ϕ_p and the volume fraction of the cells φ_{cells}. The effective diffusion coefficient is then given by Equation 15 regarding the cells as impermeable spheres.

$$\frac{D_e}{D_{e_0}} = \frac{1-\varphi_{\text{cells}}}{1+\varphi_{\text{cells}}/2} \tag{15}$$

This approach results in an effective diffusion coefficient of 3.4×10^{-10} m^2/s.

Based on the calculated data and the values obtained by the measurements, a prediction of the critical radius for oxygenation is possible. For the set of parameters on fermentation day 5 (cell number. 0.985×10^6 cell/mL) a critical radius of 250 μm was calculated. The measurements showed a maximum penetration depth of 300 μm. This difference could be explained by the inhomogeneous distribution of the cells on the carrier and the nonspherical shape of the carrier. Different cell concentrations on days 7 and 17 (0.93×10^6 c/mL and 0.55×10^6 c/mL) yielded oxygenated carrier shells of 300 μm and 430 μm respectively.

In summary the mathematical describtion supported the experimental findings.

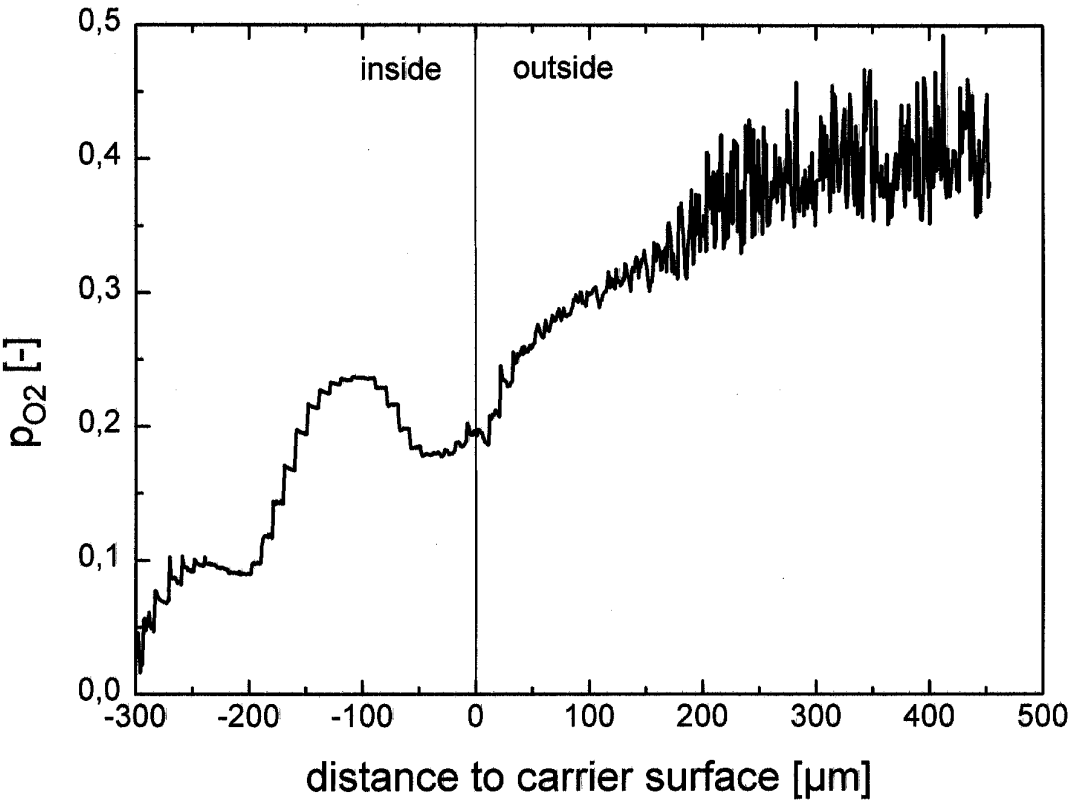

Figure 8. DO profile inside the carrier volume and near the surface. The carrier was sampled on day 5 of fermentation.

Discussion

So far, fluidized bed bioreactors using macroporous microcarriers seem to represent the most efficient cultivation method for adherent cells. Compared to fixed bed systems and Roller bottles, fluidized bed reactors showed promising properties in respect to optimal mass transfer characteristics, scale-up potential, cell-loading capacity and economy. In spite of these advantageous features, our experience gives evidence of some contradictory results.

Although glucose and glutamine as major energy sources never dropped below a limiting concentration, the metabolic activity of the population started to decrease at least after ten days of cultivation. However, toxic metabolites such as lactate and ammonium were not found to be responsible for this trend since their concentration remained low. Even the composition of amino acids was thoroughly analyzed to control a potential influence. No shortcomings could be detected in this respect either. To avoid harmful effects through mechanical stress, the linear fluid flow rate was diminished. The results showed that even very gentle mixing characteristics were able to maintain an optimal supply of nutrients and an efficient removal of toxic metabolites. No significant concentration gradients occured throughout the fluidized bed (see Table 1). Local gradients effecting the metabolism of the cells were not likely since the bulk concentrations were far from critical values and the diffusion coefficients are not as critical as in the case of oxygen (Andrews, 1988).

Although, as shown above, the medium components gave no evidence of any limitation, the fluorescent staining of the cells supported the impression of suboptimal conditions during the fermentation process. The optical examination revealed that there is a close correlation between a decreasing metabolic activity and product formation and the viability of the culture. A striking fact was, that only a layer at the surface of the microcarrier was viable, whereas cells growing *inside* the macroporous structure died after a short period of cultivation.

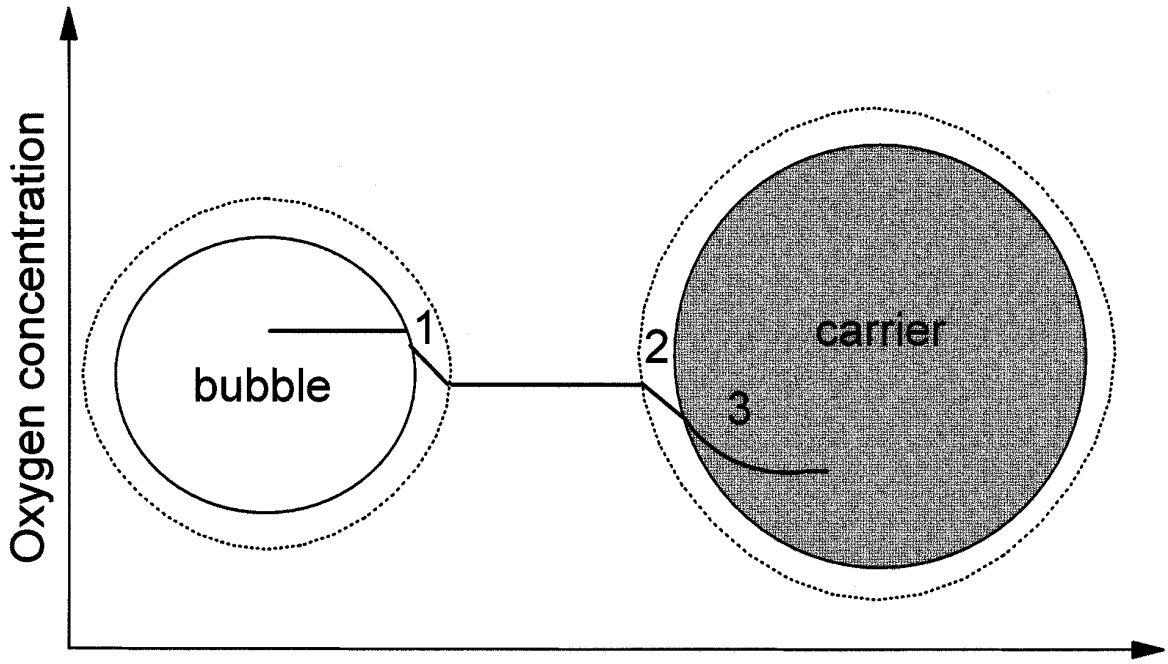

Figure 9. Schematic diagram of oxygen mass transfer from a bubble to the carrier volume.

Taking all these results into consideration, our interpretation is as follows: The growth of rC–127 on macroporous carriers is apparently limited by oxygen transfer into the carrier. The time course of the metabolic activity corresponds to that of the oxygen consumption rate. Both show a decrease after a cultivation period of 7 resp. 17 days (see Figs. 2 and 3). With the help of an oxygen microprobe, we found that in the early stage of the culture, during the exponential growth phase, a bulk liquid concentration of 40% of air saturation is apparently not sufficient. Therefore, experiments using higher initial oxygen concentrations are planned. Resistances to mass transfer occured at the surface and inside the particles, as recently mentioned by Born *et al.* (Born, 1995).

The maximum penetration depth of oxygen into colonized carriers was found to be 300 μm, which corresponds to the maximum oxygen diffusion pathway calculated by Griffiths (1990). Andrews calculated a critical radius of only 200 μm for tissue cultures using an 'effectiveness factor' as a dimensionless metabolic rate (Andrews, 1988). Compared to other results, the measured value turned out to be much lower: Chang *et al.* (1988) determined a penetration depth of 500–1000 μm for animal and plant tissue regarding their specific oxygen demand. They stated that the oxygen transfer in a microcarrier system is usually gas/liquid mass-transfer limited. Bliem *et al.* (1988) proposed a critical radius of 300–700 μm. Bignami *et al.* (1991) presented a biofilm model based on the boundary condition that an oxygen gradient between pellet surface and bulk liquid does not exist. They also distinguished an active biofilm layer near the surface and an underlying inactive radius of limited conditions. The assumption of equal concentrations in the bulk liquid and at the pellet surface could not be proven. As our results show, there is a *significant gradient* near the surface of a microsphere. Therefore, the mass transfer resistance in the laminar boundary film cannot be neglected.

Moreover, the individual morphology of the cells represents an additional barrier to mass transport into the carrier volume. The tissue structure of the cell layer at the surface covers the pores and adds to diffusion resistance. Consequently, the porous volume of the carrier cannot be colonized and the cells inside the matrix deteriorate. The 'micropump principle' introduced by Vournakis *et al.* (1989) which describes an improved environment of porous microspheres in fluidized bed bioreactors through pressure-induced pumping effects, will have little or no effect in this case.

Summarizing the results, the macroporous microcarrier is still not an optimal matrix for the stringent

adherent rC–127 cell line applied in these experiments. The main disadvantage is that it lacks a sufficient mechanical support for the cells since they are stretched across the pores. This phenomenon causes an increased sensitivity against mechanical stress and an additional resistance to mass transport into the microsphere. Therefore, the large surface area cannot be used effectively. The cell density does not reach the expected values and therefore the product yield is not satisfactory.

Alternatively, stainless steel wire springs have been established as carrier material. This matrix produced far better results. Werner *et al*. (1988) reported that the springs can be applied succesfully to the production of various products such as interferons, vaccines and monoclonal antibodies. Based on the results of this study, these systems should be considered for a more effective cultivation of rC–127 cells.

Conclusions

The results of this study lead to the following conclusions for the cultivation of rC–127 cells on macroporous microcarriers:

1. The macroporous structure of the tested carrier is not an ideal mechanical support for cell growth. rC–127 tends to form tissue-like structures which are stretched across the pores. According to that, the cells are exposed to mechanical damage.
2. No shortcomings concerning medium components could be detected. Feed strategy and fluidized bed operating conditions are able to maintain an efficient nutrient supply.
3. Decrease in metabolic activity is apparently due to oxygen limitations within the carrier. The maximum penetration depth of O_2 into Cytoline carriers colonized by rC–127 cells was measured to be 300 μm.
4. A mathematical description based on mass transport models of the oxygen mass transfer supported the experimental findings.
5. The oxygen gradient in the laminar boundary film at the surface of the microsphere cannot be neglected. Measurements showed a concentration gradient of 14% to 26% depending on the OUR.
6. Since there is a significant resistance to the oxygen transfer into the carrier, the surface area can not completely be used. Cell density and product yield of rC–127 growing on Cytoline carriers are therefore not efficient.
7. Fluorescence staining revealed that only a thin cell layer *at the surface* of the microcarrier can be kept viable. Cells inside the carrier volume which grow beneath this layer will degenerate.

Acknowledgement

Special thanks go to Gisela Seebich for her experienced performance of fluorescence staining. The support of Dieter Schuller concerning microcarrier fermentation is gratefully acknowledged.

References

Andrews G (1988) Fluidized-bed bioreactors. Biotech and Gen Eng Rev 6: 151–178

Bassi AS, Rohani S and MacDonald DG (1991) Fermentation of Cheese Whey in an immobilized-cell fluidized bed reactor. Chem Engineering Communications 103: 119–129

Baumgärtl H and Lübbers DW (1973) Platinum needle electrode for polarographic measurement of oxygen and hydrogen, in: Oxygen Supply, Verlag Urban and Schwarzenberg

Baumgärtl H and Lübbers DW (1983) Microcoaxial needle sensor for polarographic measurement of local O_2 pressure in the cellular range of living tissue. Its construction and properties, in E Gnaiger and H Forstner (eds.) Polarographic oxygen sensors, Springer Verlag, Berlin, Heidelberg, pp. 37–65

Beunink J, Baumgärtl H, Zimelka W and Rehm HJ (1989) Determination of oxygen gradients in single Ca-alginate beads by means of oxygen microelectrodes, Experientia 45: 1041–1047

Bignami L, Eramo B, Gavasci R, Ramadori R and Rolle E (1991) Modelling and experiments on fluidized-bed biofilm reactors, Water science and technology 24, No. 7: 47–58

Bliem R and Katinger H (1988) Scale-up engineering in animal cell technology: part II. TIBTECH 6: 224–230

Born C, Biselli M and Wandrey C (1995) Oxygen transfer from the gasphase to the immobilized cells in membrane aerated fluidized beds. Proceedings of the 8th meeting of JAACT, Iuzuka, Fukuoka, Japan (in press)

Brauer H (1971) Grundlagen der Einphasen- und Mehrphasenströmung. Verlag Sauerländer, Aarau and Frankfurt

Chang HN and Moo-Young M (1988) Analysis of oxygen transport in immobilized whole cells. Bioreactor immobilized enzymes and cells: fundamentals and applications: 33–51, Elsevier applied science

Deckwer W-D (1985) Reaktionstechnik in Blasensäulen. Salle-Verlag, Sauerländer-Verlag, Aarau, Frankfurt, Salzburg

Griffiths B (1990) Advances in animal cell immobilization technology. Animal Cell Biotechnology 4: 149–166

Henzler HJ and Kauling DJ (1993) Oxygenation of cell cultures. Bioproc Eng 9: 61–75

Kennard ML and Piret JM (1994) Glycolipid membrane anchored recombinant protein production from CHO cells cultured on porous microcarriers. Biotech and Bioeng 44: 45–54

Kunii D and Levenspiel O (1969) Fluidization Engineering. RE Krieger publishing company, Malabar, Florida, USA

Looby D and Griffiths JB (1990a) Immobilization of animal cells in porous carrier culture Tibtech 8: 204–209

Looby D, Griffiths JB and Mistler M (1990b) Verfahrenstechnische Aspekte der Immobilisierung von Säugerzellkulturen auf offenporigen Sintergläsern in Festbett- und Fließbettreaktoren. Chem Ing Tech 62, No. 7: 566–568

Murdin AD, Kirkby NF, Wilson R and RE Spier (1988) Immobilized Hybridomas: Oxygen diffusion, Animal cell Biotech 3:55–74

Nikolai TJ and Hu W-S (1992) Cultivation of mammalian cells on macroporous microcarriers. Enzyme Microb Technol 14, No. 3: 203–208

Özoguz G, Räbiger N and Baumgärtl H (1994) Membraneinsatz zur Erhöhung der Nitrifikationsleistung durch getrennte Substratversorgung, Bioforum 17: 129–135

Preißmann A, Bux R, Schorn P and Noé W (1994) Comparative study of the propagation of anchorage-dependent cells using different forms of macroporous microcarrier. Poster presented at the 13th meeting of ESACT, Veldhoven, The Netherlands

Riethues M, Buchholz R, Onken U, Baumgärtl H and Lübbers DW (1986) Determination of oxygen transfer from single air bubbles to liquids by oxygen microelectrodes. Chem Eng Process 20: 331–337

Riquarts H-P (1981) Strömungsprofile, Impulsaustausch und Durchmischung der flüssigen Phase in Blasensäulen. Chem Ing Tech 53: 60 ff

Vournakis JN and Runstadler PW (1989) Microenvironment: The key to improved cell culture products. Biotechnology 7: 143–145

Werner RG, Merk W and Walz F (1988) Fermentation with immobilized cell cultures. Drug Res 38, No. 2: 320–325

Westrin BA and Axelsson A (1991) Diffusion in gels containing immobilized cells: a critical review, Biotech and Bioeng 38: 439–446

Whitman WG (1923) The two film theory of gas absorption. Chem Metallurg Eng 29: 146–148

Wiesmann R (1994) Einfluß der Immobilisierung auf den Stofftransport in biotechnischen Produktionsprozessen, in: Fortschrittsberichte, VDI-Reihe 17 No. 113, VDI Verlag, Düsseldorf

Wittler R, Baumgärtl H, Lübbers DW and Schügerl K (1986) Investigations of oxygen transfer into penicillium chrysogenum pellets by microprobe measurements, Biotechnol Bioeng 28: 1024–1036

Address for correspondence: A. Preissmann, Dr. Karl Thomae GmbH (Boehringer Ingelheim), Department of Biotechnical Production, Birkendorfer Str. 65, 88397 Biberach/Riss.